Neutron Imaging of Lithium Concentration in Battery Pouch Cells

Jason B. Siegel, Xinfan Lin, Anna G. Stefanopoulou, and David Gorsich

Abstract— **This paper shows how the principle of neutron radiography can be used to quantify the critical physical state of lithium concentration across battery electrodes at steady-state conditions (after a long relaxation time or small load) as a first step in this important effort to measure in-situ battery physical states and validate electrochemical battery models. A model of the expected loss in beam intensity after passing through the different layers of a battery pouch cell is constructed based on the material densities and dimensions. This model is augmented with simulation of the neutron transmission behavior, including optical effects due to the geometric unsharpness and the detector response. The resulting model provides the basis for a comprehensive simulation of the in-situ metrology of lithium concentration in Li-ion batteries, and comparison with experimental results.** *This work was also presented as a poster at the 27th Annual Army Science Conference [1].*

I. INTRODUCTION

Battery management requires accurate prediction of bulk and the spatiotemporal Lithium (Li) concentrations. The bulk concentration is a good metric for the total available energy stored in the battery. The spatial distribution is important for predicting the available power. The minimum and maximum local concentrations of Li-ions throughout the electrode and the electrolyte solution limit the performance and longevity of the battery [2], [3]. The electrode material can be modeled as a distribution of spherical particles along the electrode, as shown in Fig. 1. The ratio of Li surface concentration over the maximum concentration represents the amount of readily available power because the surface lithium is easily removed, whereas the ions near the center of the particle are limited by the rate of diffusion to reach the surface [4], [5], [6].

Hence, our ability to control the power and fully utilize the energy from Li-ion batteries depends on physics-based and scalable battery models of the spatiotemporal variations in lithium concentration throughout the electrode and electrolyte. Although there are many distributed parameter micro-macro scale physics based models of the electrochemical reactions and mass transport phenomena occurring inside the battery, they could all benefit from measurement of the lithium concentrations for model validation. Neutron radiography offers a unique opportunity for measuring in-situ, the changes in lithium concentration and hence can be used for parameterization and validation of mathematical

J. B. Siegel is with the Dept. of Electrical and Computer Science University of Michigan Ann Arbor, MI 48109, USA `siegeljb@umich.edu`

Xinfan Lin, and Anna G. Stefanopoulou are with the Dept. of Mechanical Engineering University of Michigan Ann Arbor, MI 48109, USA `xflin@umich.edu`, `annastef@umich.edu`

David Gorsich is with the U.S. Army Tank Automotive Res, Dev & Engr Center (TARDEC) Warren, MI, 48397-5000, USA `david.gorsich@us.army.mil`
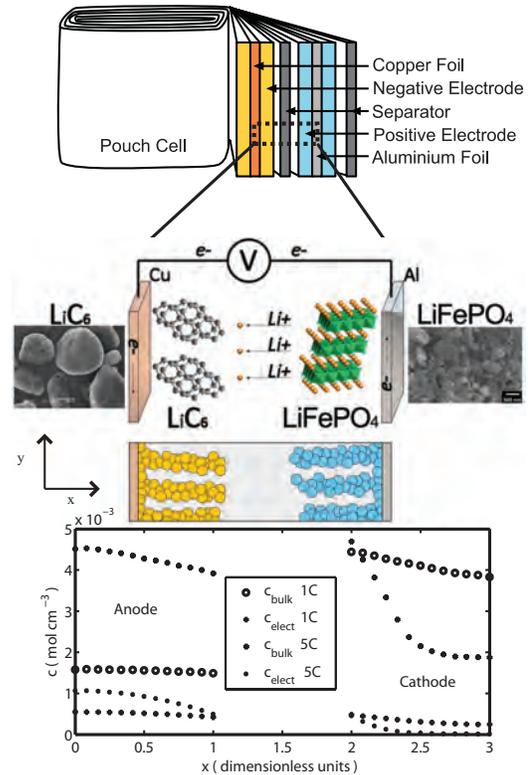
Fig. 1. The pouch cell construction used for neutron imaging is shown with an expanded view of the electrode structure. The lithium concentration distribution varies across the electrode in the solid and the electrolyte during battery discharging as a function of C-rate, using the battery model provided in Comsol.

models of Li-ion cells. Prior efforts to utilize neutron imaging resulted in only qualitative results [7], [8].

This manuscript includes data and a metrology simulation that fill the critical gap of experimental verification and availability of in-situ lithium concentration patterns in the area of lithium-ion batteries. In this paper, we investigate the capabilities of neutron imaging for *in situ* measurement of the spatial-temporal concentration of Li in a battery. We discuss the physics of the image formation process using pinhole optics, the Lambert-Beer law, and the energy dependent neutron cross sections. The pouch cell construction, shown in Fig. 1, consisting of multiple layers was imaged using the thermal neutron imaging beamline at the National Institute for Standards and Technology (NIST). Experiments were conducted with the high resolution Micro-Channel Plate (MCP) detector, which is a state of the art neutron detector at the NIST Center for Neutron Research (NCNR).

Report Documentation Page		*Form Approved* *OMB No. 0704-0188*

1. REPORT DATE **JUN 2011**	2. REPORT TYPE	3. DATES COVERED **00-00-2011 to 00-00-2011**

4. TITLE AND SUBTITLE **Neutron Imaging of Lithium Concentration in Battery Pouch Cells**	5a. CONTRACT NUMBER
	5b. GRANT NUMBER
	5c. PROGRAM ELEMENT NUMBER
6. AUTHOR(S)	5d. PROJECT NUMBER
	5e. TASK NUMBER
	5f. WORK UNIT NUMBER

7. PERFORMING ORGANIZATION NAME(S) AND ADDRESS(ES) **U.S. Army Tank Automotive Res, Dev & Engr Center (TARDEC),Warren ,MI,48397-5000**	8. PERFORMING ORGANIZATION REPORT NUMBER

9. SPONSORING/MONITORING AGENCY NAME(S) AND ADDRESS(ES)	10. SPONSOR/MONITOR'S ACRONYM(S)
	11. SPONSOR/MONITOR'S REPORT NUMBER(S)

12. DISTRIBUTION/AVAILABILITY STATEMENT
Approved for public release; distribution unlimited

13. SUPPLEMENTARY NOTES

14. ABSTRACT
This paper shows how the principle of neutron radiography can be used to quantify the critical physical state of lithium concentration across battery electrodes at steady-state conditions (after a long relaxation time or small load) as a first step in this important effort to measure in-situ battery physical states and validate electrochemical battery models. A model of the expected loss in beam intensity after passing through the different layers of a battery pouch cell is constructed based on the material densities and dimensions. This model is augmented with simulation of the neutron transmission behavior including optical effects due to the geometric unsharpness and the detector response. The resulting model provides the basis for a comprehensive simulation of the in-situ metrology of lithium concentration in Li-ion batteries, and comparison with experimental results.

15. SUBJECT TERMS

16. SECURITY CLASSIFICATION OF:			17. LIMITATION OF ABSTRACT	18. NUMBER OF PAGES	19a. NAME OF RESPONSIBLE PERSON
a. REPORT **unclassified**	b. ABSTRACT **unclassified**	c. THIS PAGE **unclassified**	**Same as Report (SAR)**	**6**	

II. Lithium Metrology

Neutron imaging is a valuable tool for in-situ measurements, similar to x-ray radiography. The change in attenuation of a neutron beam passing through a sample can be used to measure a change in the material over time. The utilization of neutron imaging for Fuel Cell (FC) liquid water metrology has been demonstrated at imaging facilities by NIST [9] and PSI [10], and advanced our understanding of the water dynamics and associated FC degradation phenomena [11], [12]. A similar approach can be applied to measure the Li movement between the positive and negative electrodes of an operating Lithium ion battery, since Li also has a large cross section for thermal neutrons. Specifically the areas shown in Fig. 2 indicate the probability of neutron interaction with atoms of various materials used in the construction of Lithium-ion Batteries. When a neutron interacts, it has a much smaller probability of reaching the detector, which leads to beam attenuation. The change in Li concentration causes a change in neutron beam intensity which reaches the detector after passing through the battery, as shown in Fig. 3. The largest change in molar concentration of lithium occurs within the intercalation materials. Hence, the change in detected beam intensity can be related to the change in Li concentration in the solid electrodes.
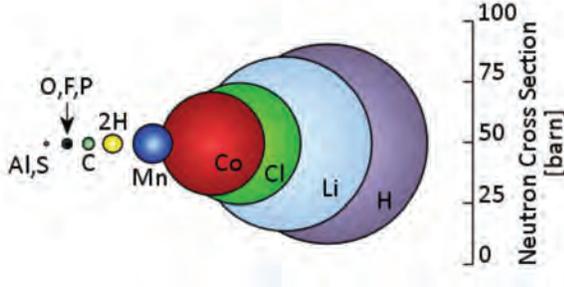
Fig. 2. Averaged total (scattering and absorbing) neutron cross-sections based on naturally occurring abundance of isotopes.

A. Principles of Neutron Imaging

The attenuation of neutron beam intensity is described by the Lambert-Beer Law

$$I = I_0 \exp(-\mu\delta) \tag{1}$$

where I_0 is the incident intensity which passes through a material of width δ (cm) with attenuation coefficient μ. Neutron interactions can occur as either scattering or absorbing or both, depending on the material. For the purpose of imaging we consider the effects of both scattering and absorption since both effects will prevent neutrons from reaching the detector, by simply adding the scattering and absorbing cross sections for each material to get an estimate of the total beam attenuation.

As a first order approximation for an object consisting of many materials the total attenuation can be calculated from the composite neutron interaction probably of each

independent material scaled with the molar concentration of that material. Since the battery is composed of many materials, we can write the total linear attenuation as the sum of two components, one which is changing over time, the lithium concentration, $c_{Li}(t)$ mol cm^{-3}, and one which remains stationary;

$$I(t) = I_0 \exp(-\sigma_{Li}c_{Li}(t)N_A\delta - \sum_{i,\, i\neq Li}\sigma_i c_i N_A\delta) \tag{2}$$

where c is the molar concentration (mol cm^{-3}), N_A is Avogadro's Number, and σ_{Li} is the neutron cross section (cm^2), shown in Fig. 2. The tabulated neutron cross sections for each element (isotope) can be found on the NCNR website [13].

Therefore the change in lithium concentration over time can be related to the change in neutron intensity. The negative logarithm of the ratio of two measurements of the beam intensity, referred to as the optical density (OD), is proportional to the change in lithium concentration

$$OD = -\ln\left(I(t_2)/I(t_1)\right)$$
$$= \sigma_{Li}N_A\delta(c_{Li}(t_2) - c_{Li}(t_1)) \propto \Delta c_{Li}. \tag{3}$$

Note, the change in optical density can only be related to a change in Lithium concentration in the solid electrode, by assuming that nothing else in the battery is changing (or moving).
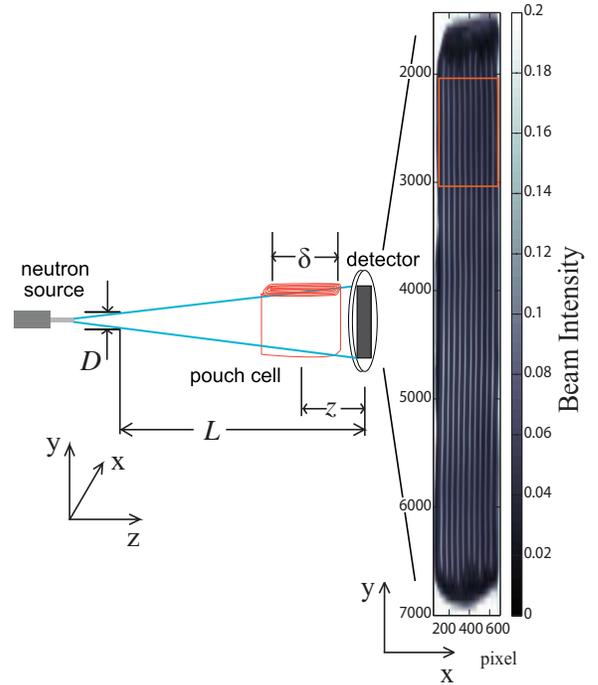
Fig. 3. (Left) Neutron imaging setup. The neutron beam is attenuated as it passes through the pouch cell to reach the detector, producing a 2-D projection of the battery onto the x-y plane. (Right) Neutron image of pouch cell

Measurement of the change in lithium ion concentration in the electrolyte is not feasible because the number density of lithium atoms in solution is too low, and hence the changes are imperceptible. This constraint of the imaging system

is not restrictive. In-fact this constraint prevents us from imaging the fast changing electrolyte concentration. On the other hand, due to the high neutron cross section of the hydrocarbon based solvents, neutron radiography has been used to see the absorption of the electrolyte into the battery electrode structure during cycling [8].

Since the image is formed by neutron counting, which is a random process, there is some uncertainty in the measurement. A reduction of the noise in the image can be achieved by increasing the exposure time of the image and counting more neutrons, but then the decreased temporal resolution may be unsuitable for imaging transient behavior such as battery charging. Another approach to reducing the measurement variance is to average many pixels together over a region with uniform characteristics, in this case lithium concentration in the electrode. By treating each pixel as an independent measurement and taking a spatial average we can achieve the same effect as increasing the exposure time at the sacrifice of in-plane resolution. Since we are interested to measure the change in lithium concentration across the electrode (in the x-direction or through plane), and the concentration along the electrode (along the y-axis or in-plane) should be uniform; averaging along the in-plane direction can be used to reduce measurement variance. Therefore the use of line-profiles, where many (approximately 1000) pixels along the y-direction are averaged together, is used for further data analysis and discussion. The line profile shown in Fig. 4(a), is calculated based on 1000 pixel average from the actual image shown in Fig. 3 as indicated by the rectangular box. As can be seen in Fig. 4(a), there is considerable variability in the transmission profile of each folded layer in the pouch cell. However, the optical density which is proportional to the change in lithium concentration is uniform across the multiple folded layers despite the considerable variability in the transmission line profile across the pouch cell as shown later in Fig. 4(b).

B. Image Formation and Capture Process

The thickness of commercial electrode materials push the resolution limit of currently available high resolution cross-strip anode Micro-Channel Plate (MCP) detectors [14], [15], [9]. Prior attempts to investigate Lithium ion batteries using neutron imaging [7] were limited by the resolution of the imaging system, but the new high resolution MCP detector, with 10 μm pore spacing, is capable of resolving features on the order of 13.5μm. The MCP has 6μm diameter pores on 10μm centers, with a 5μm pixel pitch. This high resolution detector enables the measurement of lithium concentration across the solid phase of the battery electrodes, as the typical electrode thickness is between 40-100μm [16], [6], [5].

Figure 5 shows a simulation of the resulting ideal transmission line profile according to the Lambert-Beer law Eq. (1). The cell consists of alternating double sided current collectors; LiFePO$_4$ on aluminum for the positive and carbon on copper for the negative electrodes as shown in the unwrapped pouch cell construction of Fig. 1. The electrodes are separated by a plastic separator material. The multi-
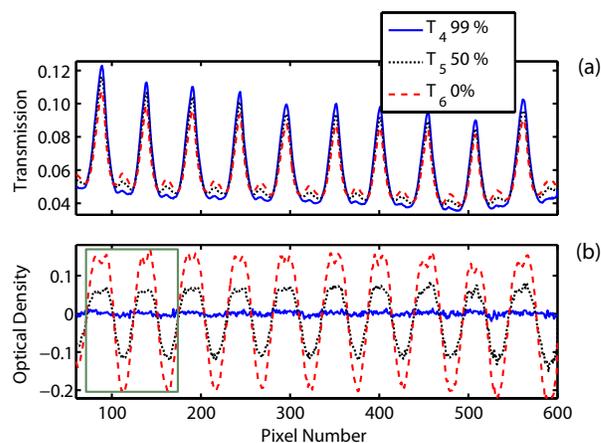
Fig. 4. Line profile of the neutron transmission at various states of charge. Each pixel is 5 μm. There is clearly variability of the neutron transmission through each fold. The optical density in the second subplot relates directly to the change in lithium concentration in the solid. Hence the mobility of Li in each fold seems to be uniform across all folds despite the observed difference in the transmission. The reference state is taken to be fully charged, so that lithium accumulation (positive values) occurs in the cathode layer when the battery is discharged relative to the reference.

layer sheets of electrode material are then folded 10 times to produce a 10 layer pouch cell shown in the neutron image of Fig. 3. The peaks in both the ideal and blurred line profiles are caused by the aluminum foil current collector which has an order of magnitude lower neutron attenuation than other materials in the pouch cell. The highest attenuation is expected to come from the separator region, since the membrane consists of plastic material that strongly attenuates neutrons, however it is not easy to identify in either the images or line-profile due to the thinness of the membrane ($\approx 25\mu$m) and proximity to the active material.

The line profile associated to the fully charged state and the material and electrode thickness is shown in Fig. 5 with the dashed line. Using modeling results from [3] a uniform Li concentration across the electrode is expected due to the low C-rate. The negative electrode thickness is approx 37 μm (each side) graphite with 10 μm copper foil backing, the positive electrode is 53 μm (each side) with 20 μm aluminum foil backing, the separators are 25 μm. The peaks in the both the ideal and blurred line profiles correspond the aluminum foil current collector which has an order of magnitude lower neutron attenuation than other materials in the pouch cell.

The image formation process introduces several artifacts changing the ideal line profile predicted by Eq. (1) shown by the square edged line into the smoother line profile. This smoothing process complicates the quantification of the lithium concentration from the detected signal. These artifacts are caused by 4 things; improper alignment of the battery with respect to the neutron beam, geometric unsharpness due to the pinhole imaging system, roughness or curvature of the object (non-parallel layers), and blurring of the signal introduced by the detector. Proper alignment of the battery layers, parallel to the neutron beam direction, is critical to produce the expected transmission line profile. If

the battery is slightly misaligned (rotation around the y-axis) the transmission line profile corresponding to the various layers in the battery may appear blurred, as shown by the line profile corresponding to the rotated image in Fig. 5, due to neutron transmission through two or more layers of the pouch cell.
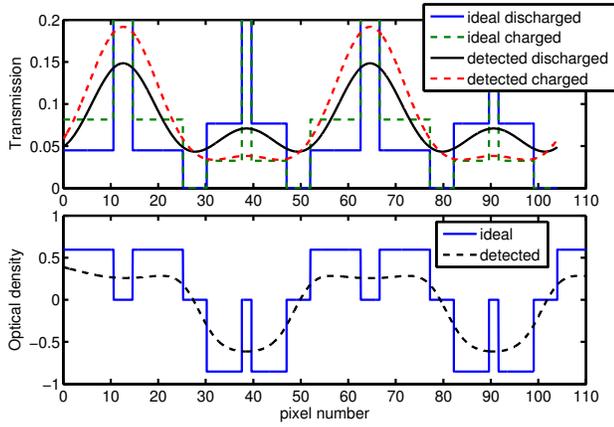
Fig. 5. Ideal simulated transmission line profile, blurred line profile and resulting optical densities in the discharged state, with the reference taken at the fully charged state.

The expected line profile is then convolved with a point spread function (PSF), to simulate the blurring of the detector, and imaging optics [9]. Deconvolution of the data, to reconstruct the ideal line profile is difficult as this would intensify the noise present in the signal [17], yielding a meaningless result. Therefore we simulate the blurring caused by the measurement system and filter the modeled transmission line profile, in order to compare the measured data with the expected results.

The geometry of the imaging setup, shown in Fig. 3, contributes to blurring of the resulting signal. This geometric unsharpness can be modeled by convolving the ideal line profile with a rectangular window of width $U_g = zD/L$, where $L/D = 3000$ is the ratio of source to detector distance over the aperture diameter, and z is the distance between the detector and the object which is imaged [9], [18]. For our experimental setup $z = 5.4$ cm, so the theoretical geometric unsharpness is $U_g = 18$ μm. The PSF corresponding to the detector can be modeled by a Gaussian kernel of width $\sigma_D = 9.2$ μm, taken from measurements of the detector [9]. The resulting simulated line profile, which accounts for the four sources of image degradation, is shown in Fig. 5. The simulated line profile with black solid line can be compared with the actual (measured) line profile in Fig. 6.

III. NEUTRON IMAGING EXPERIMENTAL RESULTS

This section describes the testing protocol used to stimulate the battery and the steady state conditions under which neutron images were acquired. Low current rates were applied to the battery in order to ensure a flat distribution of lithium concentration across the solid electrode [3], which could be easily measured and facilitate comparison with the theoretical results.

A. Experimental Procedure

The initial state of the battery was discharged, and at rest. The battery was aligned and imaged before charging at C/5 rate for 2.5 hours to 50% SOC. After another set of images was acquired, the battery was charged to 100 % SOC using a constant-current, constant-voltage (3.6V) charging algorithm. Neutron images of the battery in a known reference (fully charged) state were then acquired; where most of the mobile lithium ions are expected to be intercalated into the carbon or negative electrode. Several image frames are combined (in time) to produce an image with a very long effective exposure time (1 hour). Longer exposure times are utilized to reduce the uncertainty in the reference image from neutron counting statistics. The battery was then discharged to 50% SOC at C/5 rate and imaged during a period of rest for 1 hour with zero applied current, at time t_5. Once the imaging was completed, the discharge continued to 3V, or 0% SOC, and a final set of images was acquired under rest conditions at time t_6.

B. Expansion of electrode materials (swelling during charge)

Thermal expansion of the materials, and/or expansion of anode solid electrode material during lithium intercalation [19], requires special attention to correctly interpret the neutron radiographs. The change in lithium concentration is proportional to the negative logarithm of the ratio of two images [9], assuming nothing else within the image is moving. Movement of the active material, as suggested by the peak misalignment shown in Fig. 6 may lead to erroneous estimate of the change in lithium concentration. Therefore methods developed in subsection III-C are used to estimate and correct for the expansion/contraction of the pouch cell during charging/discharging.
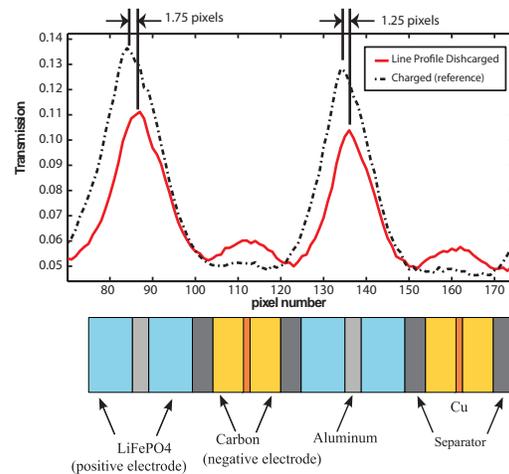
Fig. 6. The two left most peaks from the line profile of neutron transmission through the battery, from the green squares in 4, are shown with a schematic of the pouch cell showing only two folds. The total thickness of each unit battery is 260 μm, which agrees well with the average peak spacing of 52.5 pixels or 262.5 μm. Expansion of the active material during charging is visible in the peak shift. This figure shows the left-most peak which is furthest from the mounting plate and therefore subject to the greatest translational motion.

The pouch cell is secured to an aluminum fixture on the right side of the image, and therefore material expansion will produce a shift with increasing displacement (from right to left or decreasing pixel number) as the layers each move to the left, and expand. The measured peak displacements are shown in Fig. 7 and indeed follow the linearly increasing shift pattern with the distance away from the fixed mount. The average displacement corresponds to a 3% length change if attributed solely to the anode active material, which is within the range of 0-7% predicted by [19].
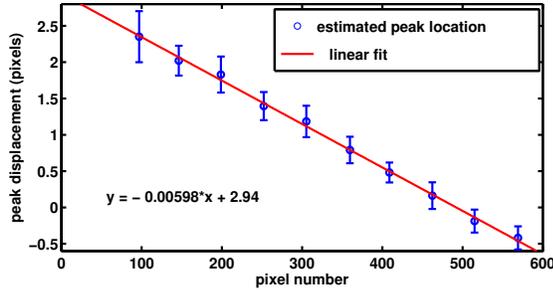
Fig. 7. Peak displacements for each of the 10 layers, from the fully charged reference state to the discharged state. Positive displacement indicates a shift in the peak location to the right during discharge. Each pixel corresponds to 5 μm. The error bars indicate 95% confidence bounds in the fit of peak location parameter $\bar{x}$.

C. Corrected Line Profiles and Optical Density

The peaks in the line profile, which correspond to the aluminum current collector for the positive electrode, provide the most well defined feature for determining the amount of translational motion present in the image. Due to the noise present in the image and in the line profile, estimation of the peak height and location is necessary, rather than simply finding the maximum value. An estimate of the peak location can be found by fitting a Gaussian kernel,

$$f(x) = \frac{a}{2\pi\sigma} \exp\left(\frac{(x-\bar{x})^2}{2\sigma^2}\right) + b \qquad (4)$$

locally to the data using least-squares algorithm with four parameters (σ, $\bar{x}$, a, b) to determine the peak location, $\bar{x}$, with sub-pixel resolution. The reference line profile is then stretched, using an affine transformation (linear interpolation) to match the peak locations. This linear scaling of the reference transmission line profile is necessary for calculating the optical density using Eq. (3), shown in Fig. 4, so that the same regions of the active material are compared and valid results can be obtained. Despite the non-uniformity in the detected transmission line profile, the optical density calculated using Eq. (3) shows uniform peak heights between pouch layers. A zoomed plot showing the optical density first two layers is shown in Fig. 8. In this figure the optical density of different material layers within the unit cell are not clearly visible. The optical density is proportional to lithium concentration; thus the only expected change in optical density should occur in the regions corresponding to the anode and cathode active material. The reference state

is taken to be fully charged, so that lithium accumulation (positive values of optical density) occurs in the cathode layer when the battery is discharged relative to the reference, and the negative electrode is losing lithium therefore the optical density decreases. The two solid lines in the optical density plot corresponding to 50% SOC are not identical. This difference, however can be explained because the first set of images (corresponding to the battery charging cycle) were taken before a change in the nuclear reactor which slightly changes the optical axis of the neutron beam.
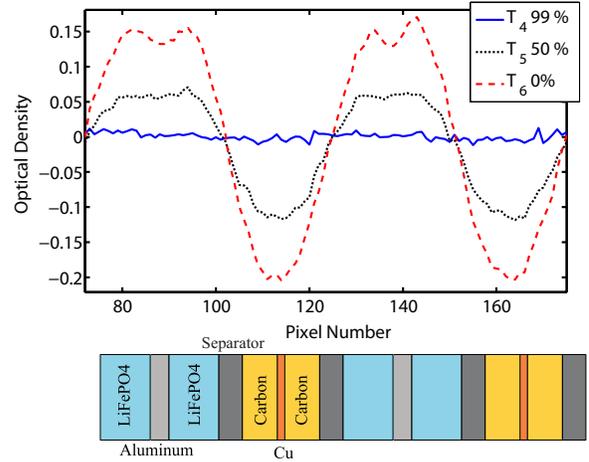
Fig. 8. Detail from 4 showing the optical density, calculated from a 4185 pixels averaged line profile of an image with a 60 minute exposure, corresponding to the first two battery folds.

IV. CONCLUSION

In order to simplify the problem and determine the quality of the metrology technique the battery is imaged during rest conditions. The electrochemical model is then used to predict to the steady state lithium distribution in the solid electrode $c_{se}(x)$, which is a constant flat profile across the electrode. The experimental results show reasonable matching with the numerical simulation for the optical density obtained from the simulation of the lithium distribution in the solid electrodes during cycling of the battery at low C-rate and imaging during steady state. The ideal line profile, corresponding to the change in lithium concentration calculated directly from the line profile using the Lambert-Beer law, does not agree with the measured data; however, accounting for the artifacts of the imaging system show much better agreement with experimental results. A high value of $\sigma_R = 30$ microns (blurring function due to rotation) as compared to the theoretical value of $\sigma_D = 9.2$ microns (blurring function due to detector), was needed to match the experimental data. The high σ_R causes increased blurring of the simulated line profile and shows better agreement with the blurred peaks in the transmission line profile, shown in Fig. 5; in particular the peak near pixel #38, corresponding to the anode active material in the discharged state, which becomes flat during charged conditions. The increased blurring observed in the neutron images may be attributed to in-plane roughness

or curvature of the battery layers, which highlights the importance of designing battery cells which are suitable for imaging.

Attempts to calculate the change in lithium concentration directly from the line profile using the Lambert-Beer law demonstrated the need to consider artifacts of the imaging system when trying to make quantitative assessments of the change in lithium concentration distribution across the electrode. Quantitative assessments of the change in lithium concentration distribution across the electrode requires calibration of the measurement tool using a Lithium Fluoride standard by NIST neutron imaging facility, which is currently in progress and once completed will allow the translation of measured optical density into the change of lithium concentration in the solid electrode. The concentration measurements can then be used to validate models for battery management.

REFERENCES

[1] J. B. Siegel, X. Lin, A. G. Stefanopoulou, and D. Gorsich, "Neutron imaging of lithium concentration for validation of li-ion battery state of charge estimation," in *27th Army Science Conference*, 2010.

[2] K. Smith, "Electrochemical control of lithium-ion batteries [applications of control]," *IEEE Contr. Syst. Mag.*, vol. 30, no. 2, pp. 18 –25, apr. 2010.

[3] D. D. Domenico, A. G. Stefanopoulou, and G. Fiengo, "Lithium-ion battery state of charge (SOC) and critical surface charge (CSC) estimation using an electrochemical model-driven extended Kalman filter," to appear in a special issue of the ASME Dynamic System Measurements and Control, 2010.

[4] S. Santhanagopalan, Q. Zhang, K. Kumaresan, and R. E. White, "Parameter estimation and life modeling of lithium-ion cells," *J. Electrochem. Soc.*, vol. 155, no. 4, pp. A345–A353, 2008.

[5] C. Speltino, D. Di Domenico, G. Fiengo, and A. Stefanopoulou, "Comparison of reduced order lithium-ion battery models for control applications," in *Proceedings of the 48th IEEE Conference on Decision and Control, 2009 held jointly with the 2009 28th ChineseControl Conference. CDC/CCC 2009.*, dec. 2009, pp. 3276 –3281.

[6] K. Smith, C. Rahn, and C.-Y. Wang, "Model-based electrochemical estimation and constraint management for pulse operation of lithium ion batteries," *IEEE T. Contr. Syst. T.*, vol. 18, no. 3, pp. 654 –663, may. 2010.

[7] M. Kamata, T. Esaka, S. Fujine, K. Yoneda, and K. Kanda, "Lithium batteries: Application of neutron radiography," *J. Power Sources*, vol. 68, no. 2, pp. 459 – 462, 1997, proceedings of the Eighth International Meeting on Lithium Batteries.

[8] M. Lanz, E. Lehmann, R. Imhof, I. Exnar, and P. Novk, "In situ neutron radiography of lithium-ion batteries during charge/discharge cycling," *J. Power Sources*, vol. 101, no. 2, pp. 177 – 181, 2001.

[9] D. S. Hussey, D. L. Jacobson, M. Arif, K. J. Coakley, and D. F. Vecchia, "In situ fuel cell water metrology at the nist neutron imaging facility," *J. Fuel Cell Sci. and Tech.*, vol. 7, no. 2, p. 021024, 2010.

[10] E. Lehmann, P. Boillat, G. Scherrer, and G. Frei, "Fuel cell studies with neutrons at the psi's neutron imaging facilities," *Nucl. Instrum. Methods Phys. Res., Sect. A*, vol. 605, no. 1-2, pp. 123 – 126, 2009.

[11] M. A. Hickner, N. P. Siegel, K. S. Chen, D. S. Hussey, D. L. Jacobson, and M. Arif, "Understanding liquid water distribution and removal phenomena in an operating pemfc via neutron radiography," *J. Electrochem. Soc.*, vol. 155, no. 3, pp. B294–B302, 2008.

[12] J. B. Siegel, D. A. McKay, A. G. Stefanopoulou, D. S. Hussey, and D. L. Jacobson, "Measurement of liquid water accumulation in a pemfc with dead-ended anode," *J. Electrochem. Soc.*, vol. 155, no. 11, pp. B1168–B1178, 2008.

[13] NIST. (2003) Neutron scattering lengths and cross sections. NIST Center for Neutron Research. [Online]. Available: http://www.ncnr.nist.gov/resources/n-lengths/list.html

[14] A. Tremsin, O. Siegmund, and J. Vallerga, "A model of high resolution cross strip readout for photon and ion counting imaging detectors," *IEEE T. Nucl. Sci.*, vol. 52, no. 5, pp. 1755 – 1759, oct. 2005.

[15] O. Siegmund, J. Vallerga, A. Tremsin, and W. Feller, "High spatial and temporal resolution neutron imaging with microchannel plate detectors," *IEEE T. Nucl. Sci.*, vol. 56, no. 3, pp. 1203 –1209, jun. 2009.

[16] M. Doyle, T. F. Fuller, and J. Newman, "Modeling of galvanostatic charge and discharge of the lithium/polymer/insertion cell," *J. Electrochem. Soc.*, vol. 140, no. 6, pp. 1526–1533, 1993.

[17] F.-X. Dupe, M. Fadili, and J. Starch, "Image deconvolution under poisson noise using sparse representations and proximal thresholding iteration," in *IEEE International Conference on Acoustics, Speech and Signal Processing, 2008. ICASSP 2008.*, mar. 2008, pp. 761 –764.

[18] D. W. A.A. Harms, *Mathematics and Physics of Neutron Radiography*. Springer, 1986.

[19] T. F. Fuller, M. Doyle, and J. Newman, "Relaxation phenomena in lithium-ion-insertion cells," *J. Electrochem. Soc.*, vol. 141, no. 4, pp. 982–990, 1994.